Journal of Power Sources 193 (2009) 276–284

Contents lists available at ScienceDirect

Journal of Power Sources

journal homepage: www.elsevier.com/locate/jpowsour

Design, building and testing of a stand alone fuel cell hybrid system

F. Segura*, E. Durán, J.M. Andújar

Department of Electronic, Computer Science and Automatic Engineering, University of Huelva, Spain

ARTICLE INFO

Article history:
Received 9 October 2008
Accepted 19 December 2008
Available online 3 January 2009

Keywords:
DC/DC power conversion
PEM fuel cell
Back-up hybrid system

ABSTRACT

This paper designs, sizes, builds and tests a stand alone fuel cell hybrid system made up of a fuel cell stack and a battery bank. This system has been sized to supply a typical telecommunication load profile, but moreover, the system can supply other profiles. For this purpose, a modular low cost electronic load bank has been designed and built. This load bank allows the power demand to be chosen by selecting different solid state relays. Moreover, a virtual instrument based on NI Labview® has been designed to select the load power demand from the computer.

1. Introduction

This work designs, builds and studies the real behaviour of a stand alone hybrid system (Fig. 1), which is made up of a PEM fuel cell stack, a battery bank and all the associated power electronics. The aim of this work is to size and build an environmental friendly back-up stand alone system (without harmful emissions, noise or grid connection). This hybrid system has been sized to supply a telecommunications station located in remote places without electrical grid nearby and with the load profile shown in Fig. 2. The outputs are 48 and 12 V-DC (see Fig. 1). The telecommunications station is connected to 48 and the 12 V-DC outputs is useful to evaluate the hybrid system under other different profile such as automotive applications. For example, in trucks, driver use a 12 V-DC connection for loads such as TV, microwave, laptop, etc.

Fuel cells are widely recognized as one of the most promising technologies to meet future power generation requirements, responding to concerns for decreasing oil consumption and dangerous CO_2 gas emissions [1,2]. One of the advantages is their modularity (they can be configured to operate with a wide range of outputs, from 50 W to 50 MW). But the dynamics of the fuel cell is limited by the hydrogen/oxygen delivery system. Therefore, an auxiliary power source with a fast response is needed. Then, a combination of a fuel cell and a battery or supercapacitor bank can form an ideal hybrid system [3]. Recently several works can be found related to fuel cell hybrid system applied to automotive, uninterrupted supply systems or auxiliary power systems [4–6].

Another characteristic which is solved with auxiliary power electronics is that PEM fuel cells supplies unregulated power [7]. According to its polarization curve, fuel cell stacks can be working at different operating points. These operating points are characterized by the voltage and current values achieved. Then, if a fuel cell stack is going to be connected to a DC load which work at constant voltage, a power conversion stage is needed. In this paper, we will called *fuel cell system* (see Fig. 1) to combination of fuel cell stack with DC/DC converter.

On the other hand, to evaluate in the laboratory the whole system behaviour under the load profile considered, a DC load controlled electronically is needed. There are multiple commercial solutions [8–12] for programmable electronic loads. But there are three main disadvantages in all of them: their high cost, their low operation range and their poor approachability, which can be seen almost like a black box. Moreover, the voltage and current values at maximum power are determined by the power contour. Ref. [13] proposes a programmable DC load, based on duty-cycle control of a DC/DC converter, whose relationships between input and output resistance are well known [14,15]. This option is a low cost interesting solution which allows selecting the load resistance, but not guaranteeing a fixed output voltage. Moreover, this solution is suitable when the load is connected to only one source.

For reasons above, a load bank controllable from a PC has been designed and built. This load bank is based on single resistive loads connected in parallel. The power demand can be decided with only selecting some solid state relays. This selection is made, to increase the security, using a virtual instrument (VI) based on NI Labview® which has been designed for this purpose. The main characteristics of the load bank are: low cost, versatility and modularity.

Several recent works focus on analyzing hybrid systems made up of one fuel cell stack [16–23]. Particularity, hybrid system supplying a remote telecommunication system are described and investigated in Refs. [24,25]. This work gives a further step, the sizes of the sources are justified, the power conversion stages are designed,

* Corresponding author. Tel.: +34 959 217385; fax: +34 959 217348.
E-mail address: francisca.segura@diesia.uhu.es (F. Segura).

0378-7753/$ – see front matter © 2008 Elsevier B.V. All rights reserved.
doi:10.1016/j.jpowsour.2008.12.111

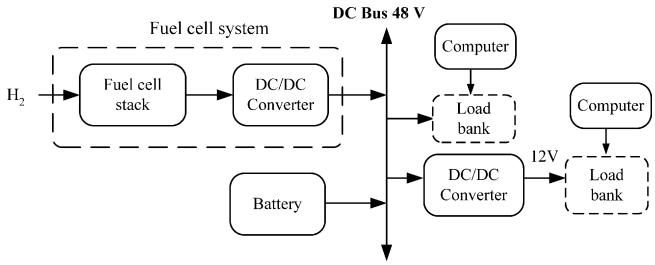

Fig. 1. Back-up fuel cell stand alone hybrid system.

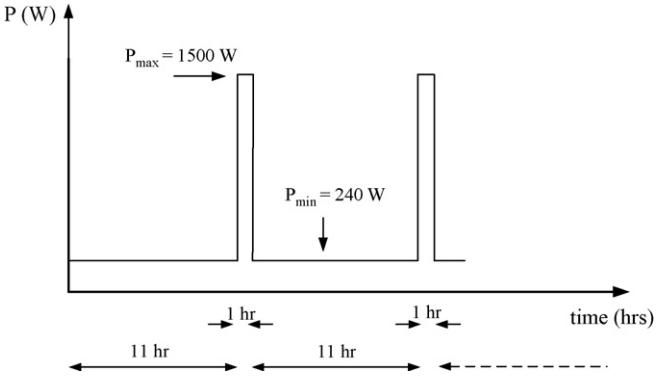

Fig. 2. Typical telecommunication load profile.

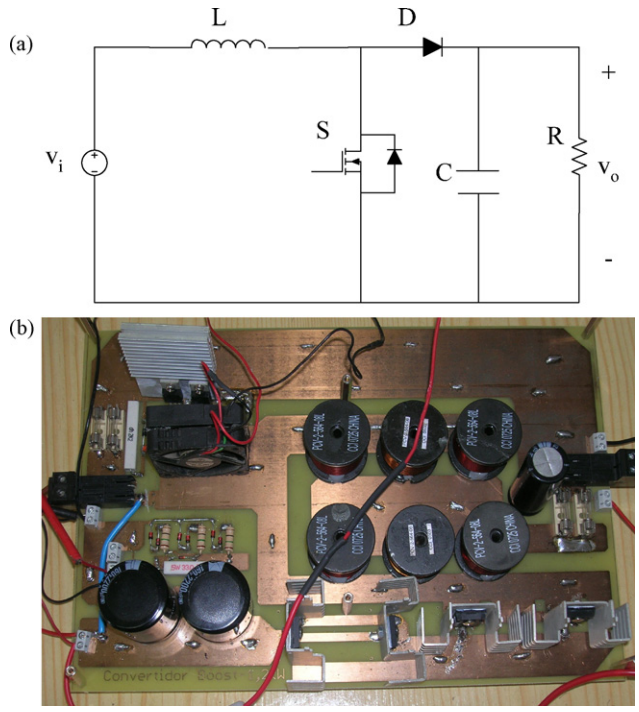

Fig. 4. (a) Boost converter scheme. (b) Boost converter implemented.

built and tested, the voltage control loop is implemented and the experimental results of the whole system are shown.

This paper is organized as follows: Section 2 contains design considerations. Taking into account the load profile, the use of a fuel cell is justified according to storage capacity, weight, flexibility, consumption and autonomy criteria. Section 3 gives a brief description of each component which integrate the whole hybrid system. Section 4 shows testing results obtained from the real hybrid system. Conclusions are presented in Section 5.

2. Design considerations

To carry out the design task, the load profile must be taken into account. Then, according to load profile shown in Fig. 2, the suitable hourly fuel cell power generation in the fuel cell/battery hybrid system is the following [26]:

(A) *Before the first power peak*: fuel cell stack (see Fig. 1) supplies a power value (P_{FC}) similar to P_{min}. Considering DC/DC converter

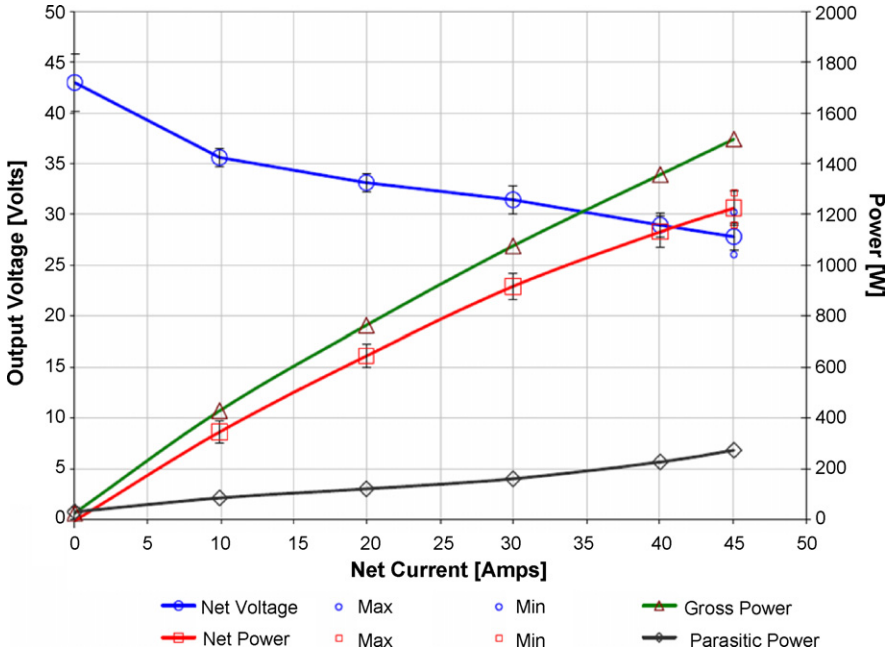

Fig. 3. Polarization and power curves for the Nexa™ module.

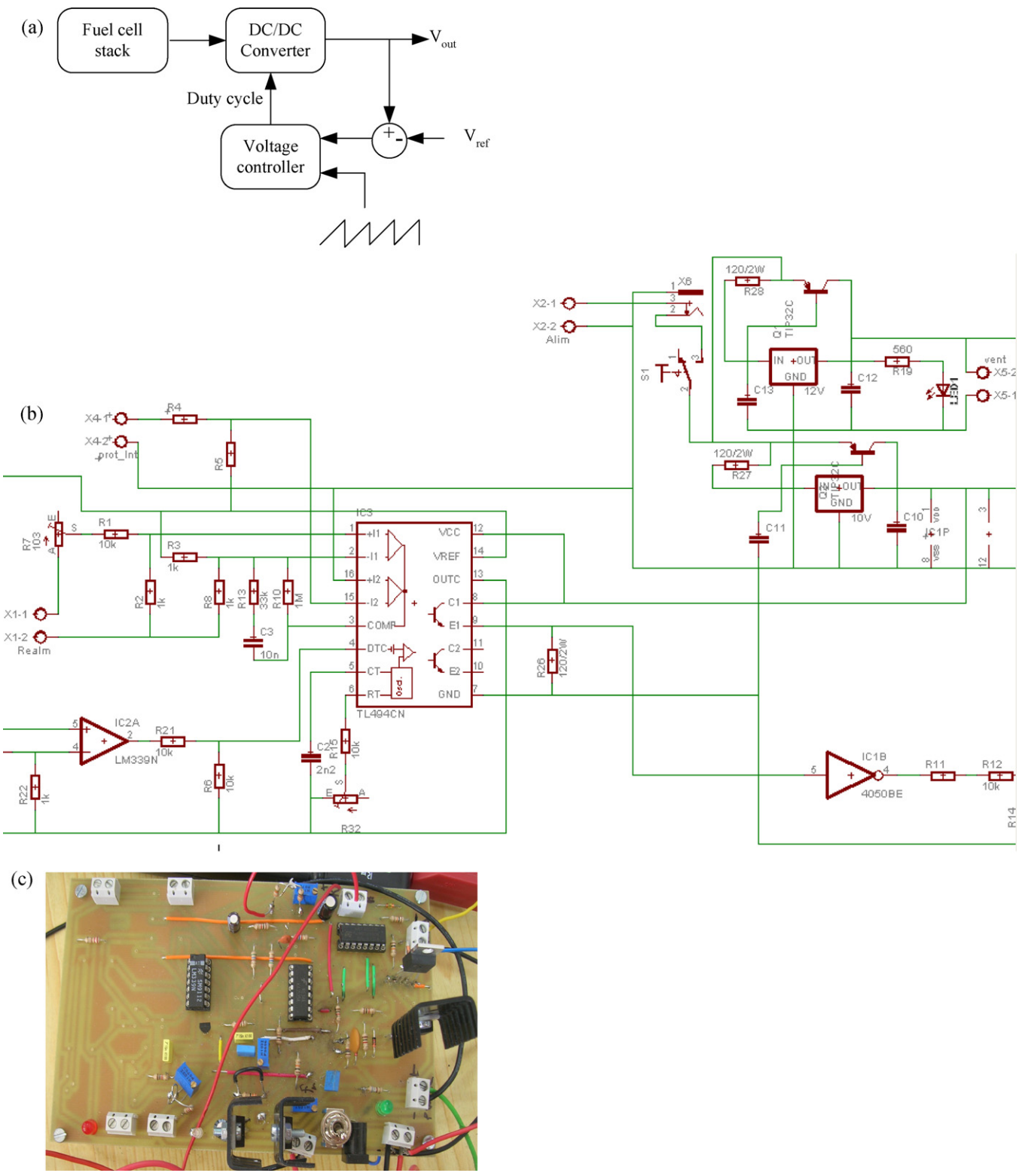

Fig. 5. (a) Voltage control loop block diagram. (b) Boost converter control board schematic. (c) Boost converter voltage control board.

efficiency (1)

$$P_{FC} = \frac{P_{\min}}{\eta_{conv}} \quad (1)$$

(B) *During power peaks*: fuel cell stack works at net power and the battery helps to supply the load demand.
(C) *Between power peaks*: fuel cell stack supplies the load demand and recharges the battery.

Then, if the value of the fuel cell stack rated power is known, it is easy to establish the energy management in the back-up power system for the specified telecommunication load profile. In general, fuel cell stack size must be selected according to the following considerations:

1. Fuel cell stack rated power must be larger than average load power in the time interval considered.

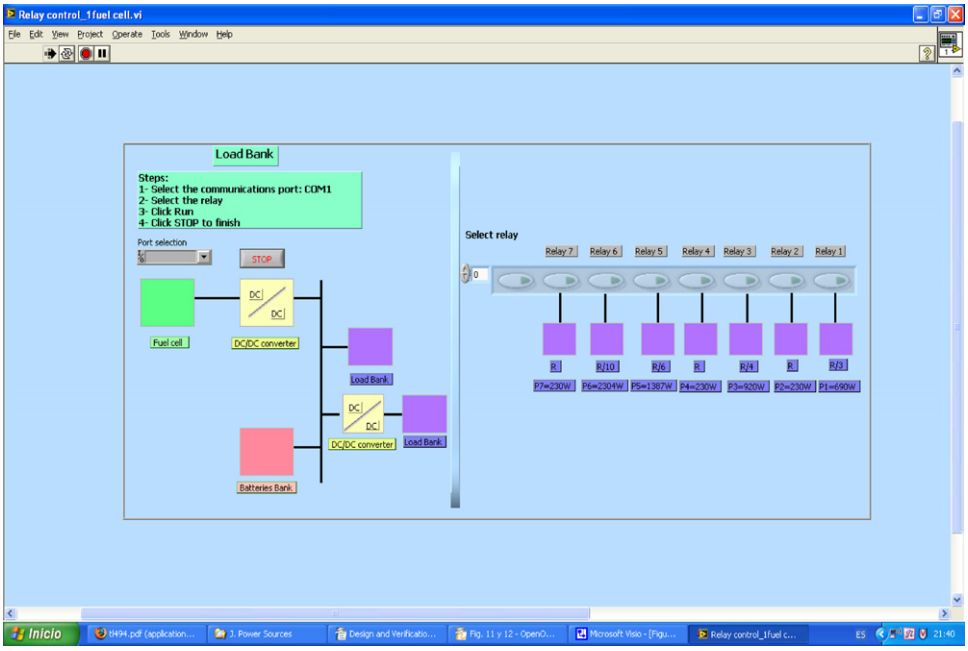

Fig. 6. Load control panel—Virtual Instrument.

2. Minimum fuel cell stack power (recommended by the manufacturer due to poor efficiency at low power levels) must be smaller than minimum load power.
3. The larger the fuel cell stack size, the higher the cost of the fuel cell stack is and the less restrictive the battery requirements are.

Therefore, an optimum fuel cell stack size must be chosen to minimize the system costs. In this practical case, according to commercial availability, the hybrid system will be made up of a Nexa™ Ballard Power module [26] (with 1.2 kW of rated power) and four GF 12 094 Y VRLA batteries. This justifies the back-up hybrid system proposed (Fig. 1). In this system, the DC bus voltage is fixed to 48 V, and then, batteries are connected in series. In Ref. [4] an exhaustive modeling task of a hybrid system similar to our system is done. Refs. [5,6] are useful works to accomplishes the system design and implementation. Developments done in Ref. [5] about the power electronics can be extended to our system, taking into account the differences in voltage and power levels. Design and packaging considerations in Ref. [6] might be a useful guide because Nexa™ power module is employed too.

The goals of this work are to design and build the whole hybrid system (including its associated power electronics) as well as to evaluate and test the real behaviour of the system.

3. Designed system description

Next, some design and operation characteristics of each component will be briefly described.

Table 1
Boost converter electrical parameters.

Device	Type	Characteristics
Mosfet-transistor	STP80NF10	2 || 100 V–80 A, 1.3 V at 25 °C
Diode	MBR6045WT	2 series 45 V–60 A, 0.75 V at 25 °C
Inductance	PCV-2-568-08	6 || 568 μH, 8 A, 90 mΩ
Capacitor	MXR 160 V–2200 μF	2|| 2200 μF, 160 V

3.1. Nexa™ PEM fuel cell power module

The Nexa™ Ballard Power system is capable of providing up to 1.2 kW unregulated DC power. The output voltage level can vary from 43 V at no load to about 26 V at full load (Fig. 3). The stack is composed of 48 single cells connected in series. The operating temperature in the stack is around 65 °C at full load. The fuel is 99.99% gas hydrogen. For more details, Ref. [27] can be consulted.

3.2. DC/DC Boost converter

To connect unregulated DC output of the fuel cell module (which varies from 43 V at no load to 26 V at full load) to a 48V-DC bus, a DC/DC Boost converter is needed (see Fig. 1).

Fig. 4(a) shows the Boost DC/DC converter electrical scheme and Fig. 4(b) shows the converter implemented for this purpose. The relation between the inductance size and input current ripple and the capacitor size and output voltage ripple are widely known [28],

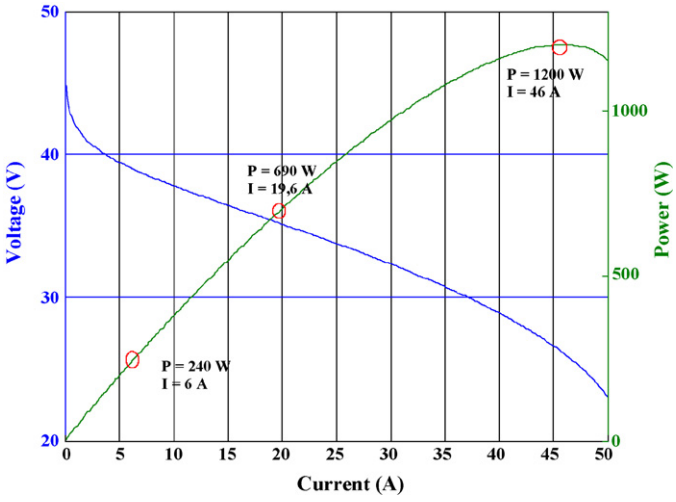

Fig. 7. Nexa™ module operating points achieved with the load bank.

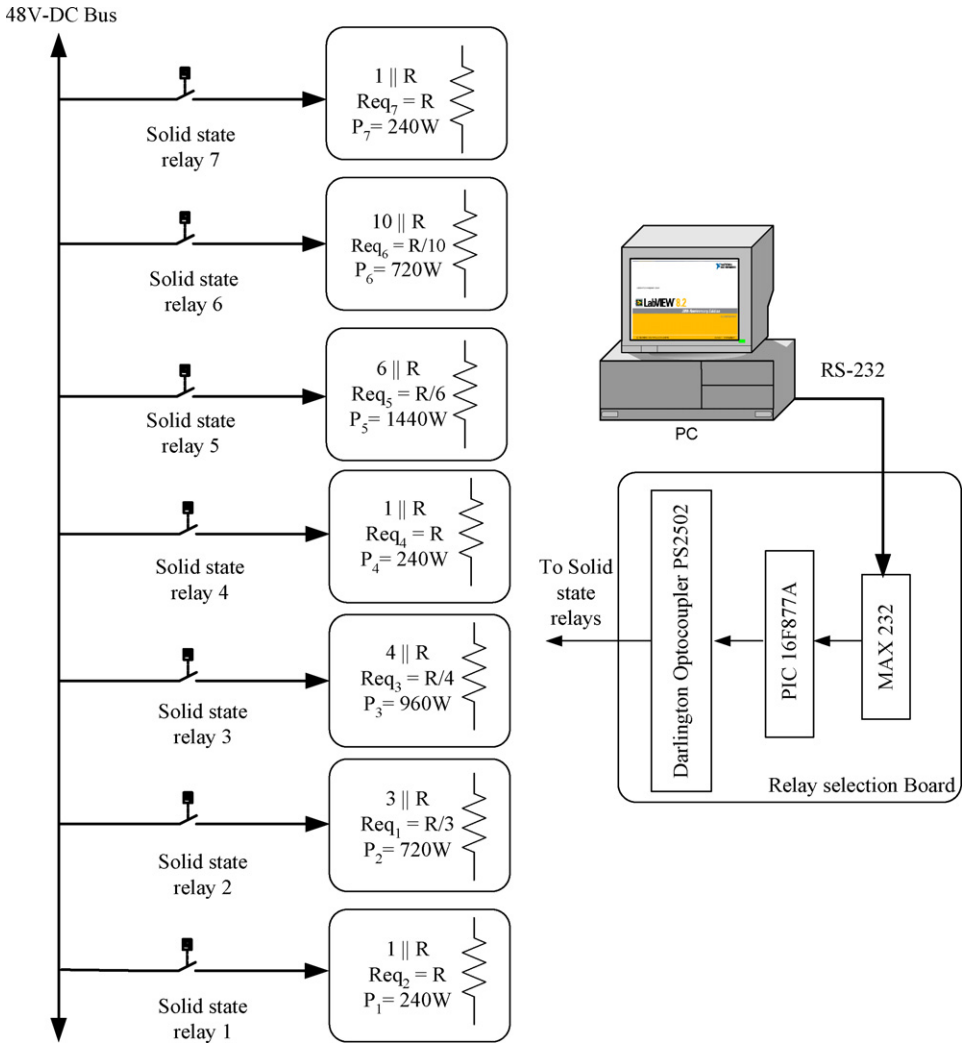

Fig. 8. Load bank scheme (communications with PC, resistance groups, number of resistances, power levels achieved).

Eqs. (2) and (3):

$$L = \frac{V_i d}{\Delta i_L f} \tag{2}$$

$$C = \frac{I_o d}{\Delta v_C f} \tag{3}$$

Electrical parameters of components used are specified in Table 1. Inductance and capacitance values are chosen to restrict the current and voltage ripple below 10%. The switching frequency is fixed to 30 kHz.

To convert the unregulated fuel cell stack output to 48 V fixed voltage, it was necessary to design and build a control system (Fig. 5(a)). The control signal (duty-cycle) is delivered from the measurement of the error between the voltage reference and the converter output voltage. The error signal is compared with a sawtooth signal. When the error signal is higher than sawtooth signal, the duty-cycle is "1" logic (high value) and the switch S (Fig. 4(a)) in "on". If the error is lower than sawtooth, the duty-cycle is "0" logic (low value) and the switch S in "off". This control system implements a voltage control loop based on TL494 [29]. This chip provides a PWM signal (duty-cycle) to control the DC/DC converter and incorporates all the functions required in the construction of a pulse-width-modulation (PWM) control circuit on a single chip. The duty-cycle is the output of a pulse-steering flip-flop. Fig. 5(b) shows the control board schematic and Fig. 5(c) show the final result.

3.3. Battery system

The battery system is a bank made up of four GF 12 094 Y VRLA batteries connected in series. From the manufacturer characteristics [30], it can be observed that the charging cycle is composed of three highlight intervals: the main charging time at constant current, the second time at constant voltage and the third time at constant current. The two last times correspond to balancing periods.

3.4. Load bank

The implementation of the load bank in our laboratory was carried out taking into account the following considerations:

Table 2
Sepic converter electrical parameters.

Device	Type	Characteristics
Mosfet-transistor	HGTG40N60B3	600 V, 70 A, 1.4 at 25 °C
Diode	MBR6045WT	3 || 45 V–60 A, 0.75 V at 25 °C
Inductance (L_1)	CH 820045	4 || 820 μH, 4.5 A, 110 mΩ
Inductance (L_2)	CH 220045	4 || 220 μH, 4.5 A, 42 mΩ
Capacitor (C_1)	TK series	330 μF, 400 V
Capacitor (C_2)	TK series	470 μF, 400 V

1. The load power demand must achieve the P_{min} and P_{max} power levels (Fig. 2), following the load profile.
2. To increase versatility and follow any other load profile, the power demand must achieve values different from P_{min} or P_{max}.
3. The load bank can be connected to system outputs (12 and 48 V).
4. To increase safety (the user does not handle any switch manually), power selection can be done by means of solid state relays ruled by a virtual instrument (Fig. 6). With this, the user sends commands from the PC to a control board, selecting which switch is open and, consequently, what power is demanded.

The load bank has been built with several resistive load groups. Each group has a sufficient number of resistive loads to achieve different power values (Fig. 7). Polarization and power curves shown in Fig. 7 are obtained by adjusting fuel cell model parameters to a Nexa™ module [31–34]. The selection of each resistive group is done by solid state relays. Fig. 8 shows how conceptually the load bank has been designed. There are seven groups of loads which have been built with a number of resistors depending on the power level to be achieved. The selection of each solid state relay is done by a control board. In the board, a MAX232 convert [35] receives signals from the PC (the commands are sent along the RS-232 wire) to TTL levels, and sends them to the microcontroller, a PIC 16F877A [36]. The microcontroller sends the commands to solid state relays through Darlington optocouplers, isolating the communication part from the power signals part. Then, when the relay 1 is switched

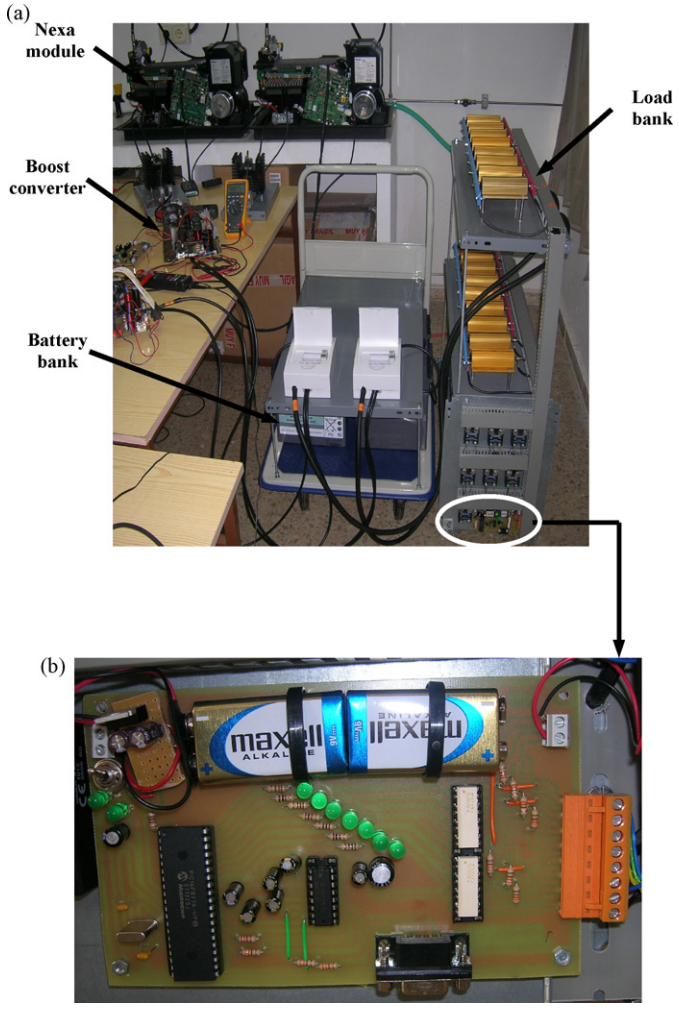

Fig. 9. (a) Load bank designed and implemented in our laboratory. (b) Load bank control board designed and implemented in our laboratory.

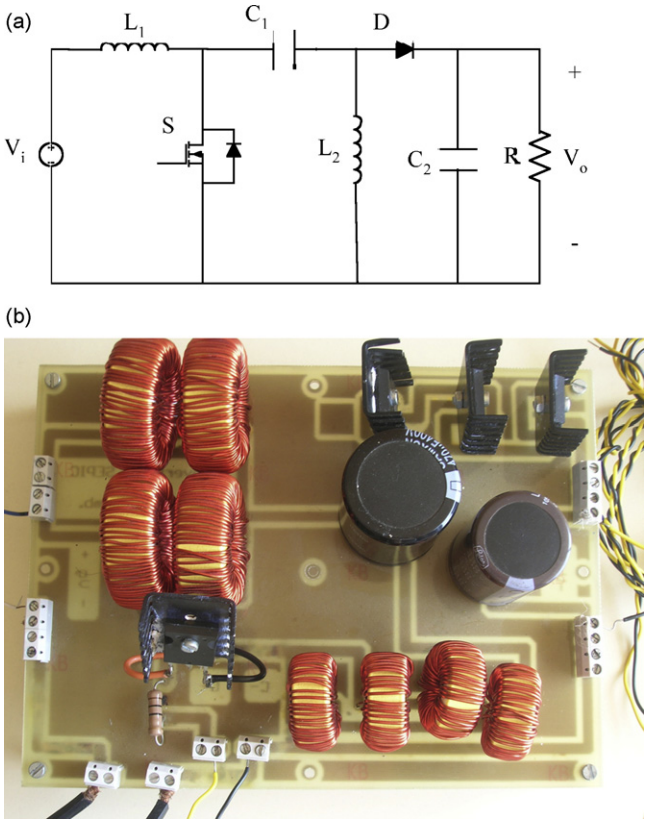

Fig. 10. (a) Sepic converter topology. (b) Sepic converter implemented.

on, the power demand is $P_1 = P_{min}$, and when relay 1, 3 and 4 are switched on, the power demand is $P_1 + P_3 + P_4 \sim P_{max}$. The rest of groups have been included to extend the load bank utility to any other load profile and to any other hybrid system (with three or more renewable sources). Fig. 9 shows the final load bank built in our laboratory connected to solid state relays, Fig. 9(a), and the relays selection board, Fig. 9(b).

3.5. DC/DC step-down converter

To convert the regulated 48V-DC bus to 12V-DC output, a DC/DC step-down converter is needed. The advantages and disadvantages of different step-down topologies are known [28]. In this sense, in Buck converter, the input current is always discontinuous because of the switch is located in series with the input source, causing great harmonic components in the current and therefore producing high input ripple and significant noise problems. Sepic converter exhibit nonpulsating input current and the output voltage is not inverted (Fig. 10(a)). Therefore, Sepic topology has been selected.

On the other hand, to control the low voltage output, a voltage control loop similar to Boost converter one has been implemented with two little differences: the resistances divisors made up of R2–R7 and R3–R8 (Fig. 5b) must have different because, now, reference value is 12 V.

The relation between the input current ripple and inductances size and the output voltage ripple and capacitors size are also known [28], Eqs. (4)–(7):

$$L_1 = \frac{V_i d}{\Delta i_{L_1} f} \tag{4}$$

$$C_1 = \frac{V_i T_{on}^2}{2\,\Delta v_{C_1} f} \tag{5}$$

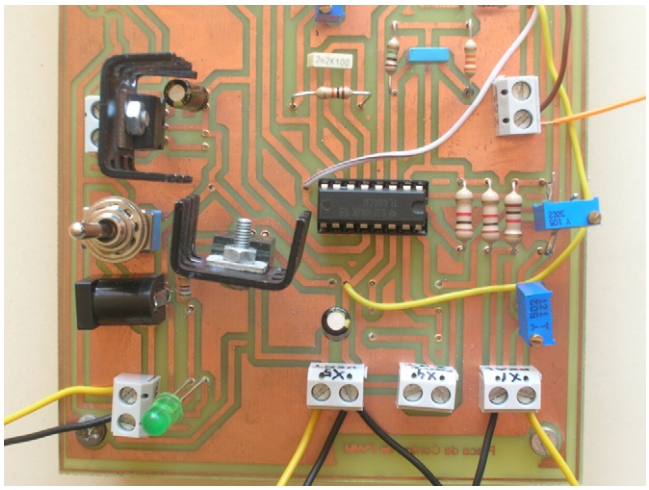

Fig. 11. Sepic converter voltage control board.

$$L_2 = \frac{V_i d}{\Delta i_{L_2} f} \tag{6}$$

$$C_2 = \frac{V_0 d}{\Delta v_{C_2} R f} \tag{7}$$

Electrical parameters of components used are specified in Table 2. Inductances and capacitances values are chosen to restrict the current and voltage ripple below 10%. The switching frequency is fixed to 20 kHz. This converter has been sizing to work a rate power of 240 W (P_{min}). In this way, experimental results can be obtained without handled high current values. Fig. 10(b) shows Sepic converter and its control board is shown in Fig. 11.

4. Experimental results

Experimental results are divided into two cases. The first one consists of connecting load bank to DC bus, where both fuel cell stack and battery bank are working together. We can check how bus voltage remains at 48 V ever under power demand steps and how when a step load occurs, the battery bank helps to fuel cell system to supply the current demanded by the load bank (see Fig. 12). The second one consists of connecting load bank to 12 V-DC output (see Fig. 13). In this case, the aim is guarantee the high and low voltage level under the whole Sepic converter operating range (0–240 W).

4.1. Load bank connected to DC bus (Fig. 12)

In this case, fuel cell system and battery bank are supplying power to DC bus. Then, when the load bank emulates the profile shown in Fig. 2, we can observe the following:

1. At low power (P_{min}), load current is $I_o = 5$ A, bus voltage is fixed to 48 V and fuel cell module voltage is $V_i = 35$ V. Taking into account Boost converter equations which related input voltage and current values to output voltage and current values:

$$V_o = \frac{V_i}{1-d}, \qquad I_o = I_i(1-d)$$

   To guarantee $V_o = 48$ V at converter output, converter duty-cycle must be $d = 0.27$. Input current, according to duty-cycle value, will be $I_i = 7$ A. Then, with the help of polarization and power curves (Fig. 3), the fuel cell operating point is known, and we can conclude fuel cell stack is the only source which supplies power to load bank.
2. At high power (P_{max}), load current is $I_o = 30$ A, bus voltage is fixed to 48 V and fuel cell voltage is 28 V. Then, according to Fig. 3, fuel cell stack works at rated power (1.2 kW). Battery bank supplies the difference between P_{max} and fuel cell rated power.

Moreover, the slow fuel cell response can be observed in Fig. 12 when a step load happens. This is the main reason to use an auxiliary power source when a fuel cell stack supplies a variable load. We can deduce that the whole system presented in Fig. 1 can satisfies the load power demand according to profile considered in Fig. 2.

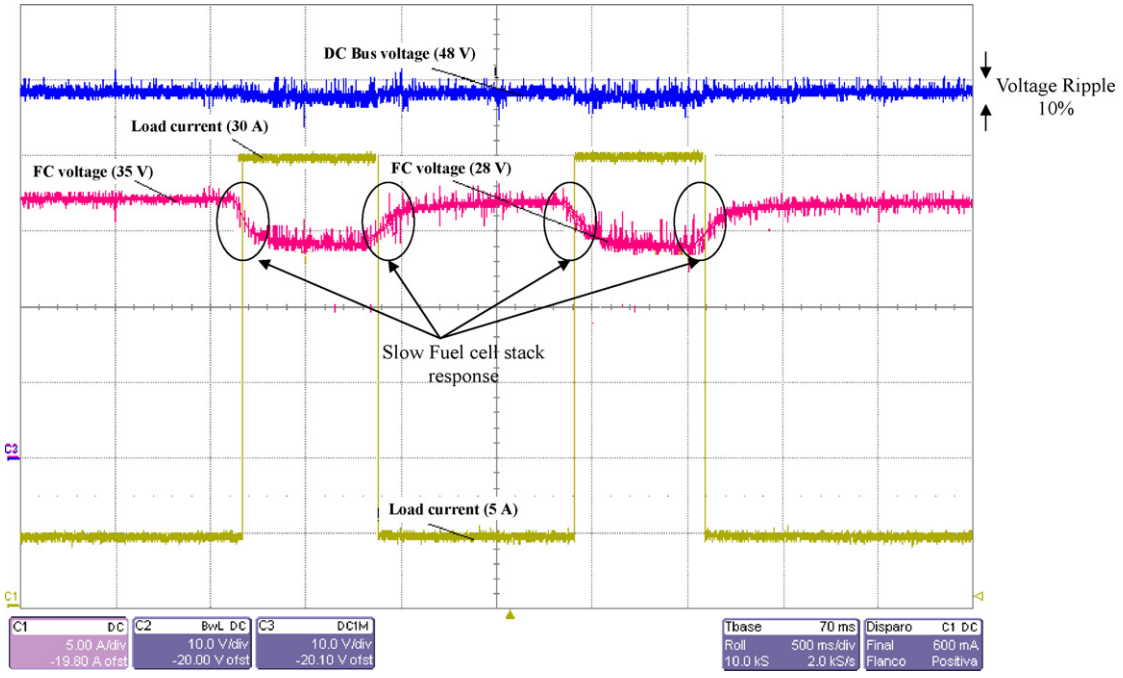

Fig. 12. Experimental results when load bank is connected to DC bus: load current (Channel C1: 5 A div^{-1}, 500 ms div^{-1}), fuel cell voltage (Channel C2: 10 V div^{-1}, 500 ms div^{-1}), bus voltage (Channel C3: 10 V div^{-1}, 500 ms div^{-1}). Oscilloscope: LeCroiy 500 MHz.

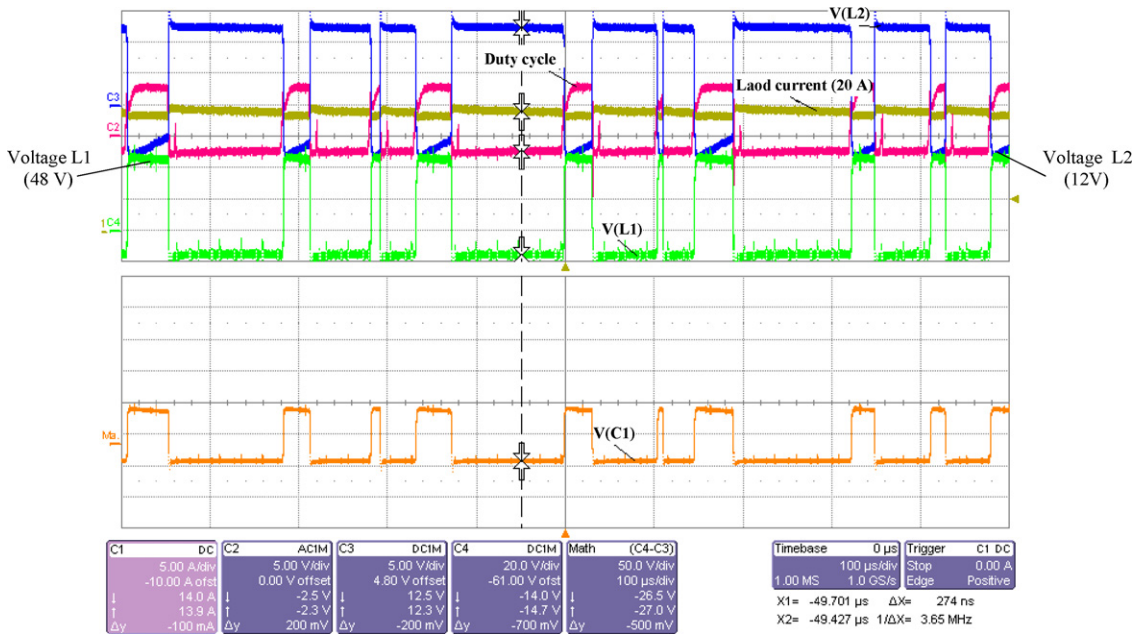

Fig. 13. Experimental results when load bank is connected to 12 V-DC output: load current (Channel C1: 5 A div^{-1}, 500 ms div^{-1}), duty-cycle (Channel C2: 5 V div^{-1}, 500 ms div^{-1}), L_1 voltage (Channel C4: 20 V div^{-1}, 500 ms div^{-1}), L_2 voltage (Channel C3: 5 V div^{-1}, 500 ms div^{-1}) and C_1 voltage (Channel C4–C3: 50 A div^{-1}, 500 ms div^{-1}). Oscilloscope: LeCroiy 500 MHz.

4.2. Load bank connected to Sepic converter output (Fig. 13)

In this case, the load bank has been connected to V_o = 12V-DC output. Because of low output voltage value and to handle secure current levels, test is going to be carried out switching on the relay 1 (P_1 = 240 W). The current demand will be I_o = 20 A and voltage control board have to adjust the Sepic converter duty-cycle to maintain output voltage to 12 V. In this case, the theoretical output current fits in the experimental value, which can be calculated by means the power Eq. (8):

$$V_o = \frac{P_1}{I_o} = \frac{240\,\text{W}}{20\,\text{A}} = 12\,\text{V} \tag{8}$$

Fig. 13 shows the load current (output current) and voltage at inductors and capacitor terminals. We can check how the voltage in inductor L_1, Fig. 10(a), reaches 48 V when the transistor is ON, and how the voltage in inductor L_2 reaches 12 V when the transistor is OFF. Then, the load power demand and voltage restrictions in DC bus and low voltage output are achieved.

It is necessary to highlight that in this last test, the load power demand is so low that the fuel cell system is the only source which is working.

5. Conclusions

This work solves a practical case related to a telecommunication system powered by a stand alone fuel cell hybrid system. The main restriction in the design process is the load profile to follow and the availability of commercial components. When different kinds of power sources and associated elements are selected, it is suitable to solve first the sizing problem by simulation. The next step has been to build the whole system. Finally, as the goal of this work is to implement a real system, it is necessary to analyze and evaluate the real behaviour of the hybrid system. This system is composed of a fuel cell module, a battery bank and all associated electronics. To fulfill the desired load profile, a resistive load bank has been designed and implemented and a virtual instrument has been programmed to control it. The system built can be used with other load profiles and different average power values.

The experimental results show the whole system works in a suitable way when different load power values are demanded to DC bus (fuel cell system works simultaneously with battery bank). Moreover, experimental results are shown when load bank is connected to 12 V output. The voltage control loop assure 48 V-bus voltage and 12 V-DC output when load steps occurs.

The designed system is an excellent testing bench; it is possible to check the performance of a system at different interconnecting points where voltage restrictions are done, the performance of different power sources and the performance of a system under different load profiles. Moreover, this system is versatile and with a simple structure. The low cost and the approachability of the controllable load bank implemented overcomes the principal restrictions of commercial electronic loads.

Acknowledgement

This work was supported by the Spanish Ministry of Science under the Project DPI2007-62336.

References

[1] K. Rajashekara, IEEE Transactions on Industrial Applications 41 (3) (2005) 682–688.
[2] T.M.W. Ellis, M.R. Von Spakovsky, D.J. Nelson, Proceeding of IEEE 89 (12) (2001) 1808–1818.
[3] A. Payman, S. Pierfederici, F. Meibody-Tabar, Energy Conversion and Management 49 (6) (2008) 1637–1644.
[4] R. Chandrasekaran, Wu Bi, T.F. Fuller, Journal of Power Sources 182 (2) (2008) 546–557.
[5] Y. Zhan, Y. Guo, J. Zhu, H. Wang, Journal of Power Sources 179 (2) (2008) 745–753.
[6] A.R. Miller, K.S. Hess, D.L. Barnes, T.L. Erickson, Journal of Power Sources 173 (2) (2007) 935–942.
[7] A.J. del Real, A. Arce, C. Bordons, Journal of Power Sources 173 (1) (2007) 310–324.
[8] Elgar, Electronic DC Load, http://www.elgar.com/products/Products_Loads.htm.
[9] Chroma Systems Solutions Inc., DC Electronic Loads, http://www.chromausa.com/electronicloads.htm.
[10] NHR Inc., AC and DC Electronic Loads for Automatic Test, http://www.electronicloads.com/.
[11] AMREL Power Products, Electronic Load, http://www.amrel.com/AMRELPowerProducts/eload_programmable_load.html.
[12] Prodigit, http://www.prodigit.com.

[13] M. Kazerani, IEEE International Symposium on Industrial Electronics (June 2007) 1015–1020.
[14] K.K. Tse, M.T. Ho, H.S. Chung, S.Y.R. Hui, IEEE Transactions on Industrial Electronics 51 (April) (2004) 410–441.
[15] E. Durán, J. Galán, J.M. Andújar, M. Sidrach-de-Cardona, EPE Journal 18 (2) (2008) 5–15.
[16] J. Samaniego, F. Alija, S. Sanz, C. Valmaseda, Fernando Frechoso, Renewable Energy 33 (5) (2008) 839–845.
[17] J. Zhenhua, G. Lijun, R.A. Dougal, IEEE Transactions on Energy Conversion 22 (2) (2007) 507–515.
[18] N.N. Barsoum, P. Vacent, First Asia International Conference on Modeling & Simulation, AMS'07, 2007, pp. 14–18.
[19] Z. Jiang, R.A. Dougal, IEEE Transactions on Industrial Electronics 53 (2006) 1094–1104.
[20] P. Thounthong, S. Rael, B. Davat, IEEE Transactions on Industrial Electronics 54 (2007) 3225–3233.
[21] S. Jemei, D. Hissel, M.C. Pera, J.M. Kauffmann, IEEE Transactions on Industrial Electronics 55 (2008) 437–447.
[22] M. Tekin, D. Hissel, M.C. Pera, J.M. Kauffmann, IEEE Transactions on Industrial Electronics 54 (2007) 595–603.
[23] J.M. Correa, F.A. Farret, L.N. Canha, M.G. Imoes, IEEE Transactions on Industrial Electronics 51 (2004) 1103–1112.
[24] S. Leva, D. Zaninelli, Electric Power Systems Research 79 (2) (2009) 316–324.
[25] P.A. Lehman, C.E. Chamberlin, J.I. Zoellick, R.A. Engel, IEEE Photovoltaic Specialists Conference 1 (2000) 1552–1555.
[26] M.J. Vasallo, F. Segura, E. Durán, J.M. Andujar, Proceedings of International Youth Conference on Energetics (IYCE'07), June 2007, pp. 215–224.
[27] Ballard Power Systems Inc., Nexa™ Power Module User's Manual, www.ballard.com/be_a_customer/power_generation/fuel_cell_powergen/nexa_power_module.
[28] M.H. Rashid, Power Electronics Handbook, Academic Press, 2001.
[29] http://focus.ti.com/docs/prod/folders/print/tl494.html.
[30] http://www.exide-technologies.ru/.
[31] J.M. Andújar, F. Segura, M. Vasallo, Renewable Energy 33 (2008) 813–826.
[32] C. Wang, H. Nehrir, R. Shaw Steven, IEEE Transactions on Energy Conversion 20 (2) (2005) 442–451.
[33] J.M. Correa, A. Farret Felix, N. Canha Luciane, G. Simoes Marcelo, IEEE Transactions on Industrial Electronics 51 (2004) 1103–1111.
[34] J.E. Larminie, A. Dicks, Fuel Cell Systems Explained, Wiley, Chichester, UK, 2000.
[35] http://focus.ti.com/lit/ds/symlink/max232.pdf.
[36] http://ww1.microchip.com/downloads/en/DeviceDoc/39582b.pdf.